VERIZONA PUBLISHER
Publishing Your Ideas

www.verizonaonlinepublishing.com
Vol: 2, Issue: 2

Material Science and Engineering with Advanced Research

A Mechanical Property, Non-Destructive Testing and Microstructural Investigation of Power Plant Mechanical Systems

S. Papanikolaou[1*], S. Maropoulos[1] and S. Makridis[2]

[1]Department of Mechanical Engineering and Industrial Design University of Applied Science of West Macedonia Kozani, Greece
[2]Department of Environmental and Natural Resources Management University of Patras, Agrinio, Greece

***Corresponding author:** S. Papanikolaou, Department of Mechanical Engineering and Industrial Design University of Applied Science of West Macedonia Kozani, Greece; Tel: +302461068218; Fax: +302461038675; E mail: sofiapapan@gmail.com

Article Type: Research, **Submission Date**: 19 May 2017, **Accepted Date:** 01 August 2017, **Published Date:** 15 August 2017.

Citation: S. Papanikolaou, S. Maropoulos and S. Makridis (2017) A Mechanical Property, Non-Destructive Testing and Microstructural Investigation of Power Plant Mechanical Systems. Mater. Sci. Eng. Adv. Res 2(2): 1-12. doi: https://doi.org/10.24218/msear.2017.24.

Coal or lignite thermal power stations are built next to the lignite mines and they are usually vast technological installations with a multitude of mechanical parts that need to be maintained and tested for life assessment. These include the excavating equipment, the ore crushers and belt conveyors, the furnace with its steam generating tubes and super heater coils, a steam drum and a steam turbine. Most of these are made of steel and other metal alloys and often fail due to normal service wear, bad maintenance, human error and poor material quality.

The ability to extend the lifetime of a plant's power plant's mechanical system beyond the original design is of very important economic and technical significance. In recent years, various techniques have been developed for inspection and control methods to be applied so that residual life in mechanical systems of power plants and welded structures can be calculated in a timely and accurate manner.

The control techniques include:

- Various non-destructive tests to examine the state of a system and the possible mechanism that causes its wear and failure
- Mechanical tests such as tensile, hardness, fatigue, impact and creep testing
- Metallographic investigation using both optical and electron microscopy
- Calculation of the operating stresses of the component, usually involving finite element analysis and a theoretical assessment of residual life depending on the wear mechanism found in the component

In the present applied research work, the above techniques are employed in case studies on various mechanical parts from the thermal plants in the region of Western Macedonia, Greece.

The purpose of the case studies was to determine the causes of mechanical failure, develop testing methods for the various parts, study the effect of material microstructure, property and processing method on part service performance and develop innovative construction methods.

Case study 1

Fatigue testing of reinforced-concrete steel bars to be used in the construction of the fifth power plant in the Region of Western Macedonia

The fatigue characteristics of reinforced-concrete steel bars are usually studied with axial fatigue tests using conventional testing machines and specimens in the as-delivered state, usually ribbed rods. The advantages of such tests include low costs and the possibility of defining test conditions precisely. However, there is a significant disadvantage related to problems connected with clamping bars in testing machines, where local stresses in bar clamping areas are responsible for the premature failure of the bars. A number of studies [1-4] contain information about various methods to prepare the grip parts of specimens usually connected with using an added layer between a specimen and a testing machine jaw and/or slight machining of specimen ends. Little information is, however, available concerning the failure mechanism of untreated bars and the effectiveness of the measures mentioned.

The study involves the fatigue testing of steel bars of various diameters to determine their fatigue strength characteristics. The problems faced during low-cycle fatigue tests of reinforced-concrete steel bars are presented and an innovative specimen preparation method is developed that will aid researchers on fatigue testing to obtain accurate test results and save on material and time. The results of mechanical tests on bars of various diameters under axial loading according to EN 10080 and EN 1421-3 are discussed and correlated with optical and scanning electron microscopy examination used to study the specimen fracture surfaces. Finite Element Modeling is employed to evaluate the effect of the newly introduced specimen preparation method on the problems faced during testing.

Methods

High cycle fatigue tests were conducted on reinforced-concrete steel 8, 12 and 20 mm diameter bars to study their behavior under axial tension loading according to EN 10080 and EN 1421-3 using a 100kN capacity Instron machine until cracking or reaching the boundary number of cycles of $2{\cdot}10^6$. The maximum and minimum loads were calculated so as to agree with the EN specifications of maximum stresses of σ_{max}=300 MPa and minimum stresses of σ_{min}=150 MPa. The load cycle frequency was set at 25 Hz.

Hardness and tensile tests were also carried out so as to determine whether the material was in agreement with the EN standards concerning concrete steel bars. The chemical composition of the material was determined using optical emission spectroscopy and the steel microstructures were studied using optical and scanning electron microscopy (SEM) to investigate the presence of inclusions that could lead to premature failure during testing. The fracture surfaces of the mechanical tests were further studied using scanning electron microscopy to obtain a better picture of the failure process.

Results and Discussion

The chemical compositions of the steel bars tested were the same at 0.22 %C, 0.57%Mn, 0.16%Si, 0.045%S and 0.024% P. The tensile test results are given in Table 1. Both are in agreement with the EN specifications so any failure during testing could not be attributed to poor quality of the material.

Table 1: Tensile Test Results

Bar diameter (mm)	Yield Strength (MPa)	Tensile Strength (MPa)	% Elongation	VPN
8	531	641	29	213
12	534	634	30	211
20	497	625	28	208

The fatigue tests of bars in the as-delivered state, that is without any preparation of the specimen grip parts, varied depending on the bar diameter Tables 2-4. The testing parameters were calculated according to EN 1421-3 and the tests were carried out at a load cycle frequency of 25 Hz for a maximum of $2{*}10^6$ cycles.

As can be seen all five bars of eight millimeter diameter withstood the required number of 2·106 cycles when tested at a frequency of 25Hz. However, when the 12 mm bars were tested a number of specimens failed usually within or very near the grip jaws (Figure 1). Moreover, all (10/10) 20 mm diameter specimens failed and this caused suspicion about the quality of the bar material.

Table 2: Fatigue Test of 8mm Diameter, 140mm Length Bars (Fmax=15.072 N, Fmin=7.536 N, Fmean=11.304 N, Famplitude=3.768 N)

Specimen	Failure (yes/no)
Φ 8-1	no
Φ 8-2	no
Φ 8-3	no
Φ 8-4	no
Φ 8-5	no

Table 3: Fatigue Test of 12mm Diameter, 168mm Length Bars (Fmax=33.912N, Fmin=16.956N, Fmean=25.434N, Famplitude=8.478N)

Specimen	Failure (yes/no)
Φ 12-1	yes934331 cycles
Φ 12-2	no
Φ 12-3	no
Φ 12-4	no
Φ 12-5	no
Φ 12-6	yes 934331 cycles
Φ 12-7	yes 964063 cycles
Φ 12-8	no

Table 4: Fatigue Test of 20mm Diameter, 280mm Length Bars (Fmax =94.200, Fmin=47.100N, Fmean=70.650, Famplitude=23.550N)

Specimen	Failure(yes/no)
Φ 1-20	yes 1088570 cycles
Φ 2-20	yes 1854310 cycles
Φ 3-20	yes 1115141 cycles
Φ 4-20	yes 675589 cycles
Φ 5-20	yes759420 cycles

Figure 1: Premature failure within or near grip jaws

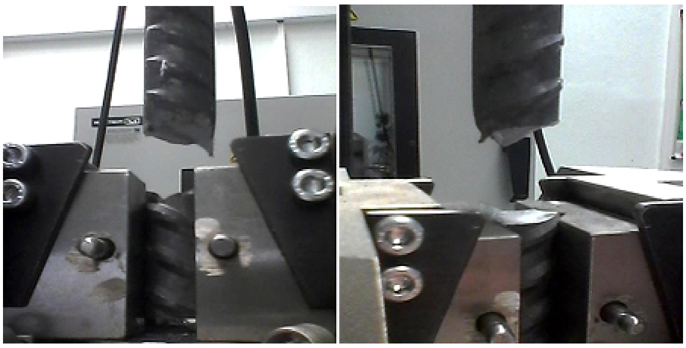

To exclude any such possibility the steel microstructures were studied using optical microscopy (Figure 2). As can be seen all diameter bars exhibited a ferrite - pearlite microstructure and no martensite or other phases were present that could account for the premature failure observed.

As expected, the fracture surface observed using scanning

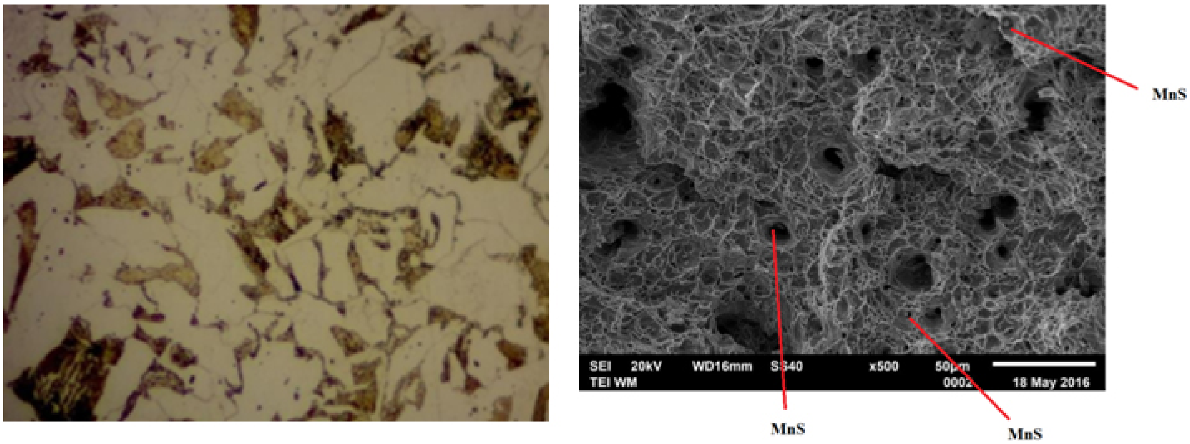

Figure 2: Steel microstructure and the ductile fracture surfaces observed using SEM showing voids and some manganese sulphide inclusions

microscopy revealed the presence of voids and manganese sulphide inclusions (Figure 2) but this cannot by itself explain why premature fracture occurred only in the over 12 mm diameter bars. Studying the literature showed that fatigue strength of concrete steel is diameter dependent [1,7-9]. Steel bars of smaller diameter exhibit higher fatigue strength than steel bars of the same quality but bigger diameter. In German standards for concrete steel a gradual reduction in the requirements for fatigue strength is reported and in BS 4449 [9] the specifications differ depending on group diameter.

In the present study the results appear to agree with the above and originally the difference in fatigue strength of the 12 and 20 mm bars in relation to that of the 8 mm ones was attributed to their larger diameters. However, a closer look at the bibliography [2-4,10-12] reveals that premature failure inside or close to the fatigue machine grips is a common problem with fatigue testing of reinforcing bars. This is due to the difficulties related to the fact that fatigue cracks are usually generated in the area where test specimens are fixed in the jaws of a testing machine, i.e. where significant notches are present. Thus, the results of such tests cannot be regarded as reliable and should or may be rejected according to the EN 1421-3.

Tilly [2] reports information about numerous attempts to properly prepare the grip parts of specimens so as to eliminate the problem of crack initiation in the grip part of the specimens; such attempts were always connected with using an additional layer between a specimen and a testing machine jaw. He [2] mentions the use of leather belts wrapped around the specimen grip part, low melting point metallic fillings, resins and aluminium pads. However, Tilly [2] does not provide any information concerning the effectiveness of the measures mentioned.

Krzysztof Krasnowski [3] mentions a successful method that was used to eliminate the problem but does not give any information of the steps taken. In addition, in the NordTest method for fatigue testing of concrete reinforcement steel bars [4] four different methods for preparing the grip parts of specimens are described in detail. However, they all seem rather complicated and/or time consuming.

In order to locally change stresses in the specimen grip area and to make the notches caused by the jaws too small to lead to the premature failure the following technique was used with surprising success in the present study. For the 20 mm diameter bars, firstly, a 50 mm length of the specimen ends was turned to 19.5 and 21.5mm diameter, respectively, until the relief on the surface was almost completely removed. There was also a 4 mm long curved part machined past the grip part (Figure 3). This resulted in a larger surface area being gripped by the machine jaws and eliminated the applied stress concentrating on only four or five points that may cause failure. Then, approximately 0.5 mm of aluminium, 5 cm wide, tape was wrapped around the specimen ends to reduce the depth of the notches caused on the specimen surface by the machine jaws part (Figure 3).

Figure 3: Machined specimen ends and specimen ends wrapped with aluminium tape

The fatigue test results of such specimens showed that none of the required five, as per EN 1421-3, failed. The same specimen end preparation method was applied to 22mm diameter bars and again no failure was observed on fatigue testing. Therefore, the problem with specimen failure was not due to material quality but specimen surface morphology that results in stress concentration and notch creation caused by the machine jaws as was proven by the finite element analysis that follows.

The geometry of an "as received" bar, as well as that of a treated one was digitized using a 3D scanner (SLS 2 DAVID Vision Systems) and the resulting *.stl file was imported into the pre-processing software ANSA (by Beta CAE Systems).

The verification of the model was largely based on the development of a mesh independent grid [13,14], generated in ANSA. Convergence studies were conducted up to a 2% results deviation indicated the optimum mesh density in terms of processing time and results. The structure of the employed validation process (trend validation) emphasized on the evaluation of theoretical scenarios allowing a comparative evaluation of the two scenarios under the applied tensile load.

Although the use of nonlinear properties is preferable to determine possible failure mechanisms at high plasticity [15], linear elastic properties were applied [13] for both scenarios, as this comparative analysis was meant to serve as an indication of critical stress concentrations that might occur during loading. The model was then imported into ANSYS (ANSYS® Academic Research, Release 15) with a non-linear solver formulation and subjected to an axisymmetric tensile load. A summary of the results obtained can be seen in Figure 4.

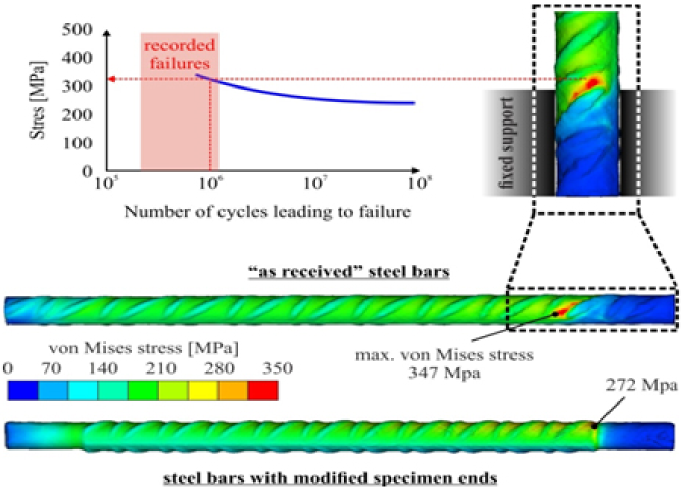

Figure 4: Comparison of developing stress fields on the as received and treated bar

Finite Element models have been widely accepted as effective in the evaluation of wear propagation [16] and failure [17] of mechanical components. As can be seen, the developing max. von Mises stress in the "as received" bar is recorded just above the tester's grip. This can be attributed to the surface area of the bar being in contact with the grip, which is lower when compared to the modified one, as the bar's surface protrusions minimize the bar/grip interface. As a result, the "as received" bar develops a max. von Mises stress which is 27,5% higher than the one observed in the modified one. According to the Smith diagram, in the top left part of Figure 4, this increase is capable of leading to failure at about 10^6 cycles, a behavior that coincides well with the experimental results.

Conclusions

High cycle fatigue tests conducted on reinforced-concrete steel ribbed rods in accordance with the specifications in EN 10080 are difficult to perform due to premature failure appearing within or near grip jaws. The specimen preparation method described above will aid researchers on fatigue testing to obtain accurate test results and save on material and time.

Case Study 2

A failure analysis investigation of a transmission precision roller chain

Failure of heavy duty precision chains has frequently caused concern to engineers as its appearance is often linked with extensive damage to industrial machinery and equipment and occasionally serious accidents [18-25]. Failure modes of chains are normal wear, roller cracking and fatigue, besides failure due to poor pin bush interference and assembly error [26]. Chain fatigue failure mostly occurs in link plates and is due to repeated tensile cyclic loading [26,27]. Chain life in general is influenced by lubricant, method of lubrication, relative hardness of pin and bush, dimensional and geometric tolerances, surface finish of pin and bush, type of assembly, preloading, and working conditions [27].

In the present study a metallurgical failure analysis investigation of a 100 HE simplex roller chain was carried out using a combination of mechanical testing, and optical and scanning microscopy. Fatigue tests on several parts of the chain revealed a diminished fatigue life caused mainly by stress corrosion cracking due to bad maintenance. The metallographic investigation confirmed the existence of defects and micro cracks and revealed the consequent crack propagation.

Methods

The present study involves a failure investigation of an ISO 110 HE transmission roller chain component of a bucket truck that failed during service causing a serious accident. Fatigue tests according to ISO 15654:2015 [28] were conducted on samples taken from the chain in order to determine its dynamic strength. In addition, fatigue tests were carried out on samples taken from similar chains that had been in operation for the same length of time as the chain under investigation as well as samples from an unused chain of the same type. Tensile tests were conducted according to ISO 606 [29] on various chain samples in order to determine its tensile strength properties and compare these with the values given in the standard for the specific type of chain.

The chemical composition of the various chain components was determined using optical emission spectrometry. Optical and Scanning Electron Microscopy were used to study the microstructures involved.

Results and Discussion

Chemical composition and microstructures: The chemical analysis of the chain components showed that the material is carbon steel of average quality since the sulphur and phosphorus content are 0.05% and 0.04% respectively. The microstructural investigation revealed a quenched and tempered martensitic microstructure present in all chain components.

Mechanical tests: The tensile tests results showed that the material complied with the tensile strength specifications set in ISO 606. The fatigue test results are shown in Table 5. Failure was observed in samples 1 and 3 both parts of the chain that failed during service. In sample 1 fracture occurred in the side plates of the pitch within the jigs and is not to be taken into consideration according to ISO 15654:2015. In sample 3, fracture occurred in one of the pins and the side plate attached to it. All the other samples tested withstood the $3x10^6$ cycles required by the test standard.

Fractography: The fracture surfaces of the samples that failed during fatigue testing were studied extensively with optical and scanning electron microscopy. Figure 5 shows the characteristic fatigue fracture surface appearance of the 10 mm wide pin and the side plate of sample 3. A heavily corroded band, approximately 5 mm and 2 mm wide, respectively, is observed in both. In addition, the pin seems to have a 0.2 mm corroded band on the opposite side and a number of vertical to this, 0.9 mm long, 0.05 mm wide, zones.

The fracture surfaces of the pin as observed with the SEM are shown in Figures 6-8. There is an initial band where wear has created a 420 μm wide crack, Figure 6, along half the pin perimeter. This is followed by a 5 mm wide area exhibiting heavy corrosion, Figure 7.

The heavily corroded band is followed by an area exhibiting partial corrosion followed by a 4 mm wide band exhibiting the characteristic ductile fracture surface appearance showing voids some of which contained particles that were found to be manganese sulphide when analysed with the EDS facility, Figure 8. Near the opposite end to the initial crack side of the pin some corrosion was again observed.

The fracture surfaces of the side plate as observed with the SEM are shown in Figure 5, 9-11. As with the pin, in one of the side plate sides there is an initial 2mm wide area, exhibiting heavy corrosion followed by a 1 mm wide area exhibiting partial corrosion, Figure 5. Numerous fine fatigue cracks are observed in both of the above areas, Figure 9.

Then follows an un-oxidised area where intergranular fracture is quite evident, Figure 10, and finally in the opposite side there is again a 0.4 mm corroded band with vertical "strings" of corrosion towards the centre of the fracture surface, Figure 11.

Table 5: Fatigue Tests on ISO 100HE And 100H Chains

Sample	Minimum UTS, Fu(kN)	Test force Fd (kN)	Max force Fmax (kN)	Min force Fmin (kN)	Test Frequency (Hz)	No. of cycles	Failure (YES/NO)
1	104	16	18,96	3,5	30	782.616	YES
2	104	16	18,96	3,5	30	$3*10^6$	NO
3	104	16	18,96	3,5	30	260.526,5	YES
4	104	16	18,96	3,5	30	$3*10^6$	NO
5	104	16	18,96	3,5	30	$3*10^6$	NO
6	87	16	17,63	2	30	$3*10^6$	NO

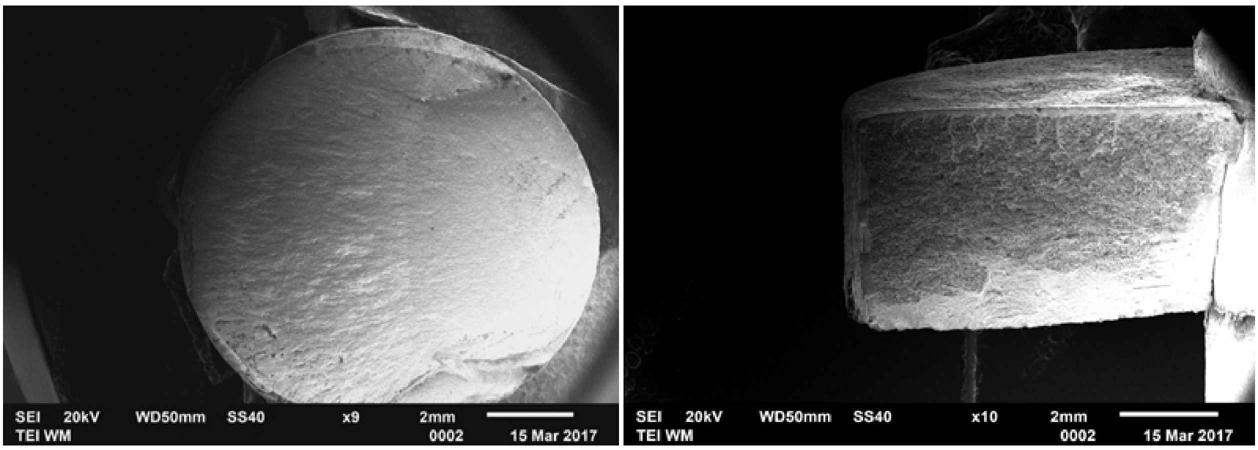

Figure 5: SEM fracture surface photograph of the pin and the side plate of sample 3

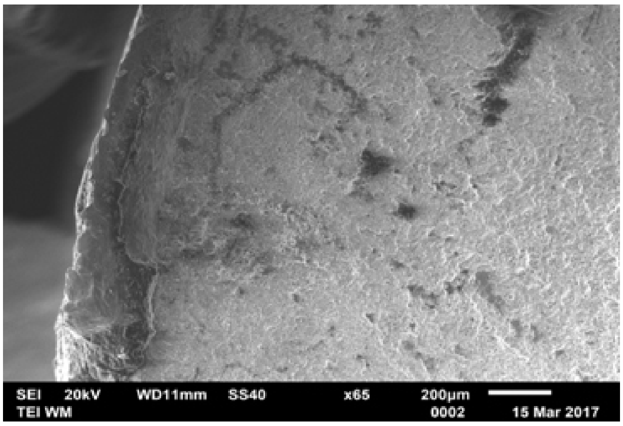

Figure 6: SEM photographs of pin fracture surface exhibiting a wide crack

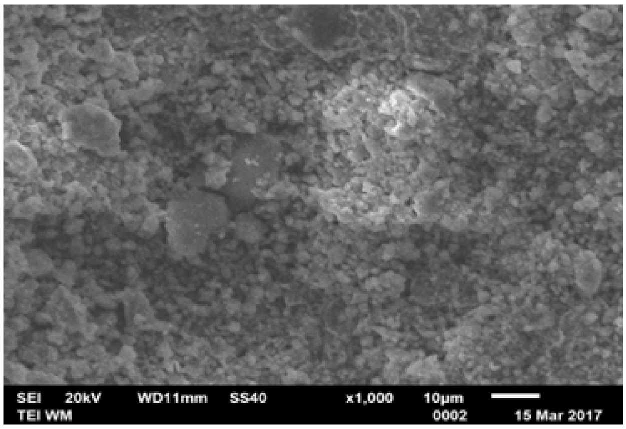

Figure 7: A 5 mm wide area exhibiting heavy corrosion

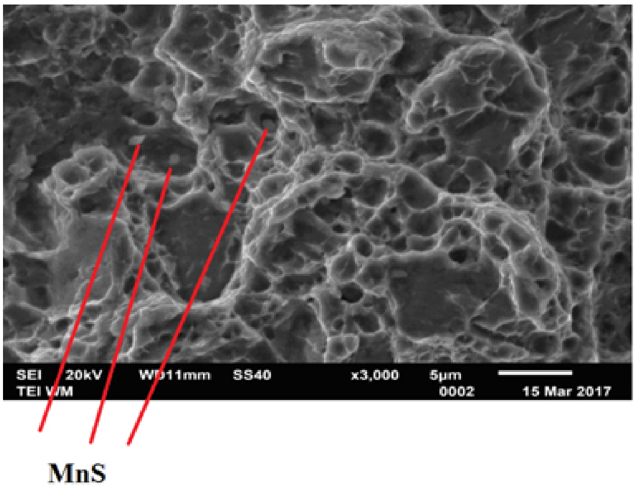

Figure 8: Ductile fracture appearance showing voids and MnS particles

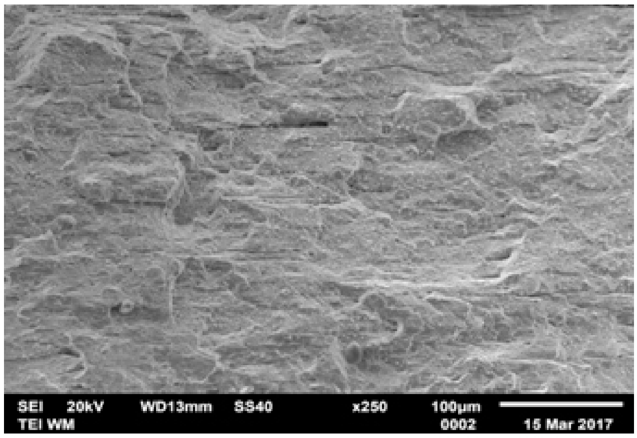

Figure 9: Fine cracks in the fracture surface of the side plate

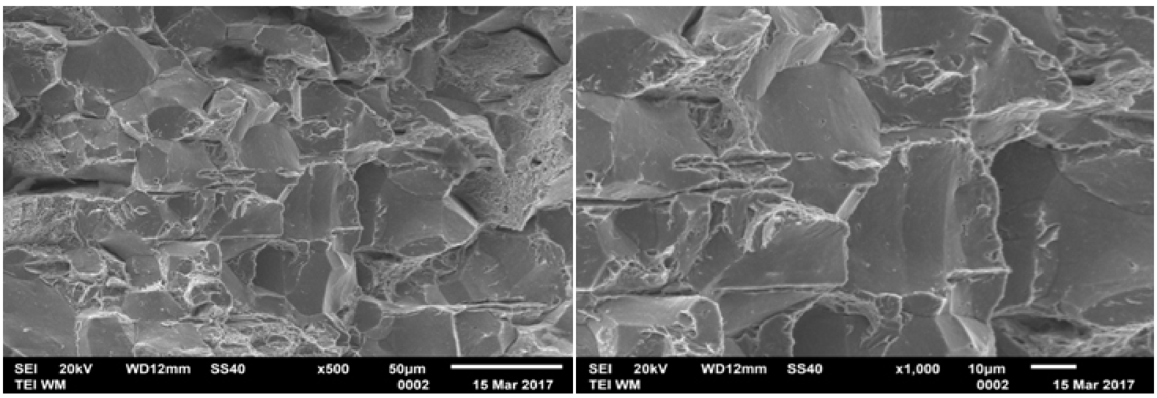

Figure 10: Intergranular fracture in the un-oxidised area of the side plate fracture surface

The fracture surface of the side plate of sample 1 that failed within the jigs was examined in order to investigate whether intergranular fracture appeared in it as well. A mixed ductile - brittle fracture appearance was observed, Figure 12. Most of the surface exhibited a brittle fracture appearance where intergranular fracture in a big number of grains appeared, Figure 13.

The three most common ways that a chain may fail are tensile, fatigue and wear [30]. In a tensile failure, the chain is pulled apart due to overloading. In a fatigue failure, the chain is loaded below the yield strength until microscopic cracks develop in the link plates and grow until the chain fails. In a wear failure, material is removed by a combination of sliding, abrasion or

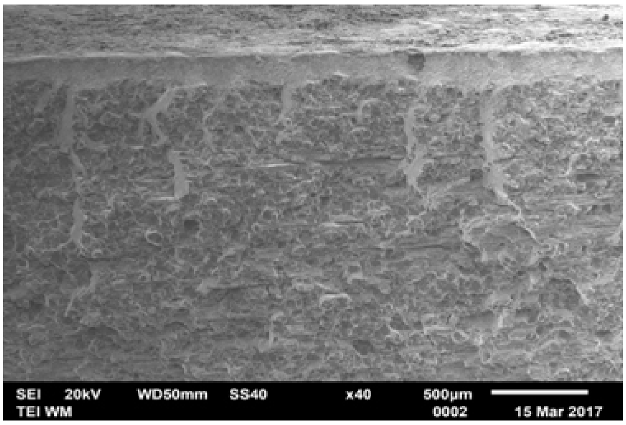

Figure 11: Corroded band with vertical "strings" of corrosion and long fine cracks

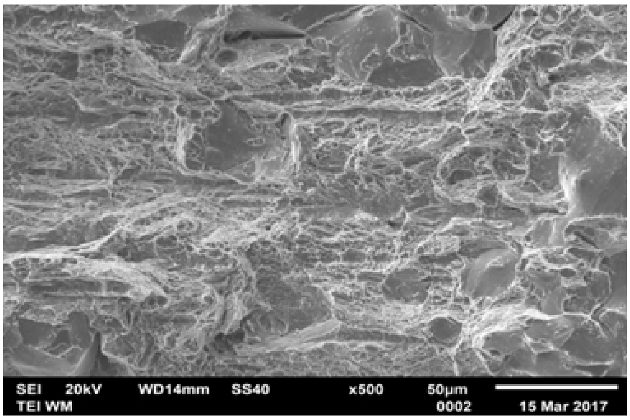

Figure 12: Ductile - brittle fracture appearance

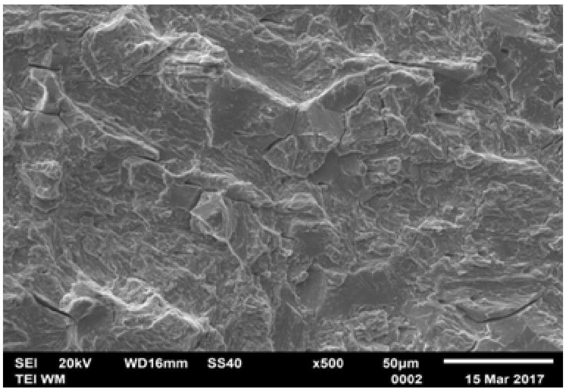

Figure 13: Intergranular fracture in a number of grains

corrosion until the chain parts do not function properly or the remaining material is so thin that the chain breaks. When a chain is operating under load, outer surface of pins and inner surface of bushings slide against each other due to articulation, thereby causing wear [31]. Due to continuous articulation movement, wear can occur in every contact cycle causing cumulative wear and consequent chain elongation.

In the present work the fracture surface investigation leads to the conclusion that the causes of failure of the chain pin are at least three. Normal wear caused by poor or no lubrication of the chain resulted in a 420 μm wide crack being formed at the pin surface. Proper chain lubrication has been proven to reduce the wear coefficient by 150% [31] and increase chain life by as much as 100 times [30]. In the present case, it is believed that once an initial crack was formed stress corrosion cracking took over, virtually eating up material thus leaving only a mere 3 to 4 mm of unaffected material having to carry the applied loads. Then fatigue crack initiation and propagation took over until final pin breakage occurred. In the case of the side plates an additional reason caused failure. The partial intergranular fracture observed is believed to be the result of temper embrittlement resulting in phosphorus segregation on grain boundaries frequently observed in steels [32,33].

Conclusions

Poor lubrication caused extensive wear to the pins surface in the chain pitches. In addition, corrosion resulted in material loss of the pins. Fatigue cracks developed in pins and side plates leading to failure. Some intergranular fracture was observed in hardened side plates probably due to temper embrittlement.

Case Study 3

Construction of a modified welded metal beam and the effect of processing on its mechanical behavior

Metal buildings constitute an alternative way of construction that offers a number of advantages as they are built faster and allow the use of smaller cross-sections in slabs and beams. The use of steel beams for the construction of the load bearing structure of a building is based on the study and design of the "composite plates", which in accordance with the provisions of Eurocode 4 includes two stages, the "construction phase" and the "operational phase". During the construction phase, i.e. before the hardening of concrete, the estimated static system has to be able to receive the tension that the concrete creates and other loads from paving, while during the operational phase, the metal part and concrete act together as a single plate with a weight of about 500kg/m^2. In addition to loads received from the metal mesh of the structure there are planning restrictions for the installation of hydraulic and electrical networks of the building for which, to date, there is no prediction during the construction phase.

The present work involves the study of the mechanical behaviour of a modified IPE 200 metal beam, one of the most common commercial beams, used in the construction of metal buildings, in order to provide for its incorporation in the initial stages of assembling a metal building [40-42]. The modification of beam IRE200 requires heat treatment and welding using conventional welding methods. Prior to a thorough investigation of the modified beam's behavior, ultrasonic non-destructive testing (UT) of the welded parts is deemed necessary [35-37]. UT will determine the integrity of the welded joints in the construction phase, contributing to the quality and safety of the metal building [38,39]. A number of welded parts from a modified IRE200 beam were inspected with an industrial ultrasound apparatus in order to detect for any discontinuities present. Then only quality welds were selected for a further study of the mechanical behaviour of the beam and they were subjected to tensile testing. The experimental results were introduced in finite element software (ANSYS Workbench 14.5) which was used for the simulation of the beam's behaviour under bending stresses [34]. The conclusions derived from the study of the modified beam are encouraging and permit its use in the construction of metal buildings under certain conditions.

Methods

Material and Cutting process: The beam material was St37, which is widely used in industrial applications, and a CNC PAC machine equipped with an air gas Thermal Dynamics torch (PCH/M-120) was used for the cutting process.

The parameters, with which the machine was set to cut for each set of experiments, are given in Table 6. Each parameter can take three different values, so that processing the experiment in various ranges of values can be possible.

Table 6: Cutting Parameters Design

No	Process parameters		Units	Level 1	Level 2	Level 3
1	A	Cutting speed	m/min	1	2.5	4
2	B	Arc ampere	amp	30	70	110
3	C	Pierce height	mm	3.3	4.8	6.4
4	D	Torch standoff distance	mm	3.3	6.4	9.5

Within the framework of the project an IPE 200 cross-section was selected and processed as shown in Figure 14. Specifically, the original cross-section was cut in the transverse axis, along the cutting profile of Figure 14 and then re-welded using automated submerged arc welding. Then, the effect of welding on the mechanical properties of the beam was investigated and the results were used in the simulation of its behavior under foreseeable operating conditions.

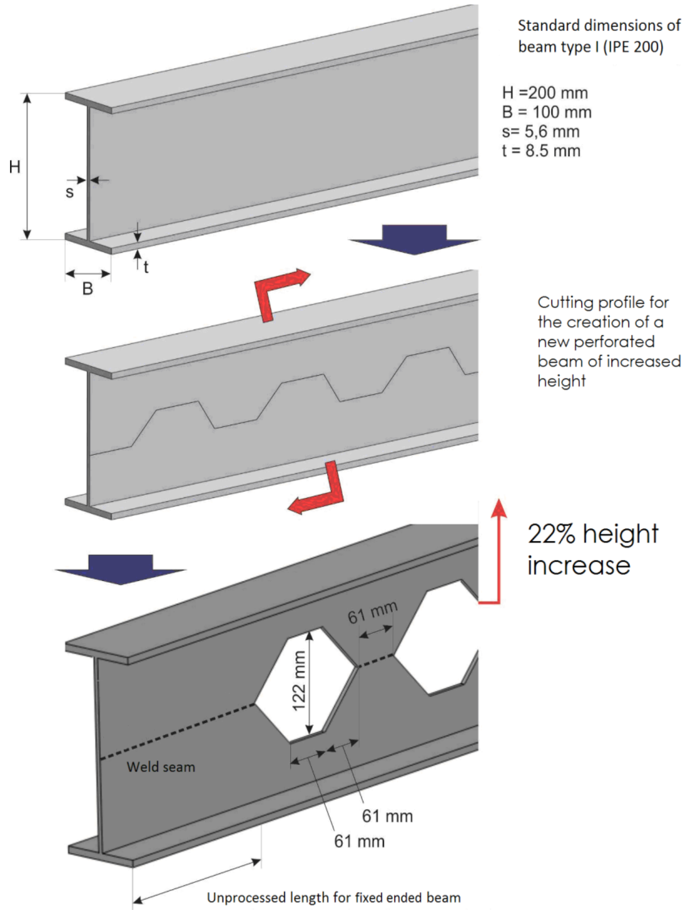

Figure 14: Manufacturing process for the modified IPE 200 beam

Non Destructive Testing: Seven welded specimens were selected to study the behavior of the modified IPE200 beam. The first inspection was performed by visual inspection followed by a manual magnetic particle (MT) examination to detect surface breakage defects and sub-surface defects up to 3mm below the surface in the 5.6mm thick welded steel specimens. The magnetic test was performed using Yokes KarlDeutch (Type: 3446.230, voltage 230V, frequency 50-60Hz and 3A current) using liquid magnetic particles aerosol and white aerosol, but no surface defects were found.

An ultrasonic test method was then used to inspect the quality of welds and find any sub-surface defects present. Scanning was carried out using the Ultrasonic Flaw Detector KarlDeutch (Digital Echograph, Type: 1090.301) using a vertical beam sensor (KarlDeutch 0°, single, 4MHz, 10mm) in the base metal region. The scanning was continued in the corner area, the bath and the angle of the welding head with Angular Beam Sensors 60° (KarlDeutch 60°, simple, 4MHz, 10mm) and 70° (SIUI 70°, simple, 4MHz, 10mm). Scan sensitivity is defined as the first rear echo at 100% of the screen. The standards used for the inspection of welded specimens were ISO 17640: 2010, ISO 5817: 2003. Preliminary checks were also performed to ensure the validity of the calibration of the machine prior to its use for ultrasonic testing.

The UT test showed that two of the seven specimens had defects and were discarded. The defects in the problematic welds were in the root and the welding bath. In particular, there was a defect in sample 1 in the weld root and in sample 2 there were defects in the bath area.

Tensile tests: In order to quantify the change in the mechanical properties of the treated beam, tensile specimens were machined from a welded section of the beam, and in particular from the five welded samples UT tested which showed quality welds, Figure 15. These samples were then compared with as received samples of the same material.

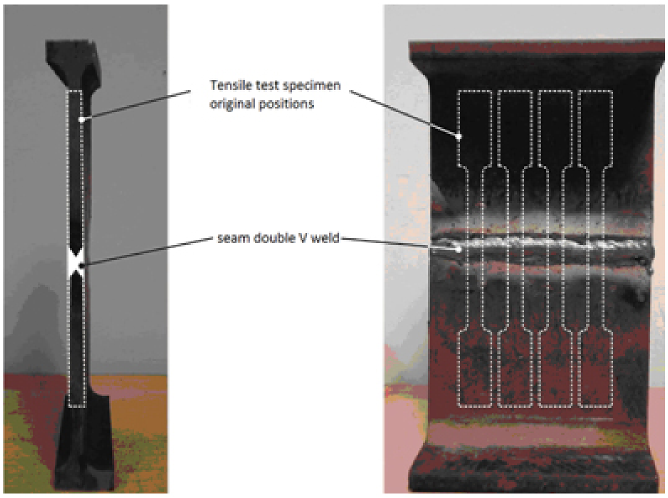

Figure 15: Method of producing welded tensile specimens

The results of the tensile tests carried out using a high precision machine (INSTRON 5980) showed that the welding treatment resulted in an increase in the mechanical strength of the test pieces by 20% and a lower % elongation. It is noteworthy that the treatment seems to leave virtually unaffected the modulus of elasticity of the beam material.

Finite element analysis: The mechanical properties calculated on the basis of the tensile experiments were introduced into finite element software (ANSYS Workbench 14.5), followed by the discretization of the geometry of the beam to be analyzed. Characteristic values of the grids taken into account are given in Table 7.

Table 7: Qualitative Data for the Grid Of Finite Elements

Qualitative data	IPE 200	**Modified** IPE 200
Number of finite elements	66354	64263
min Itemsize	0,29 cm	2,9 cm
max Item size	5.8 cm	5.8 cm
Minimum side length	0,85 cm	0,56 cm
Finite element growth rate	1,815	1,85

The uniformity of the mesh created is illustrated in Figure 16 for both the un-welded and the treated beam. As can be seen, the height of the beam, the so-called percentage "rib", increased by 22% while retaining its weight and having holes inserted which may affect its ability to pick up loads, which will then be determined by the finite element method.

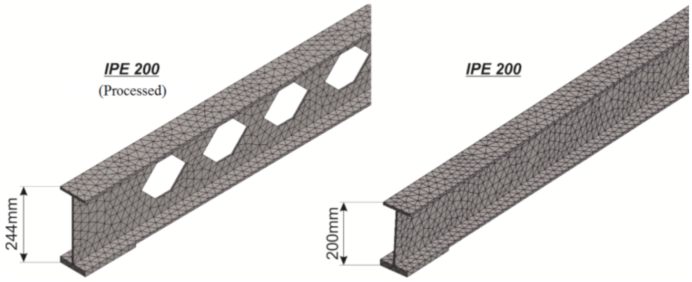

Figure 16: Differentiation of beams and finite element partitioning

For the purposes of this study, the bending stress scenario illustrated in Figure 17 was simulated. The beam was supported at both ends at a distance of 20m, simulating a fairly large opening. Complete beam coverage was adopted for an axial length of 20cm, while a uniform load of 500kg / m2 (5 MPa) was distributed to its top surface.

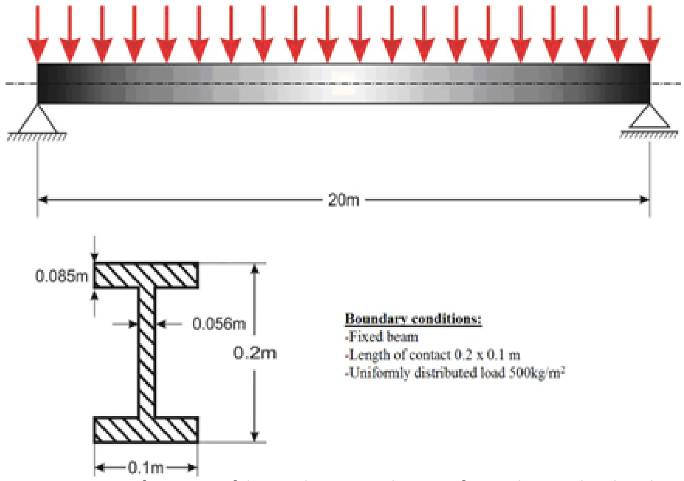

Figure 17: Definition of boundary conditions for solving the loading scenario

The simulation was based on linear-elastic properties and two criteria were compared for the mechanical response of the beams, the growing stress field and the maximum calculated deformations of the beam.

Results and Discussion

The simulation results are illustrated in the next two figures. The developing stress fields for the loading scenario are shown in Figure 18 for the unprocessed commercial section IPE200, while in Figure 19 for the processed cross section. It is interesting that the maximum stresses develop in both cases in the support area of the beam and not in the middle of it. This is due to the fact that the beam restraints limit the potential movement / deformation of the beam and therefore the growing stresses increase by 47.5%.

This, however, is local and does not cause concern, since in both cases it is clearly below the yield point of the material. In the middle of the beam there is an increase in beam load of 37.5%, which is not a large increase, considering the fact that the thermal treatment of the beam (as a result of welding) increases the mechanical strength by about 20%.

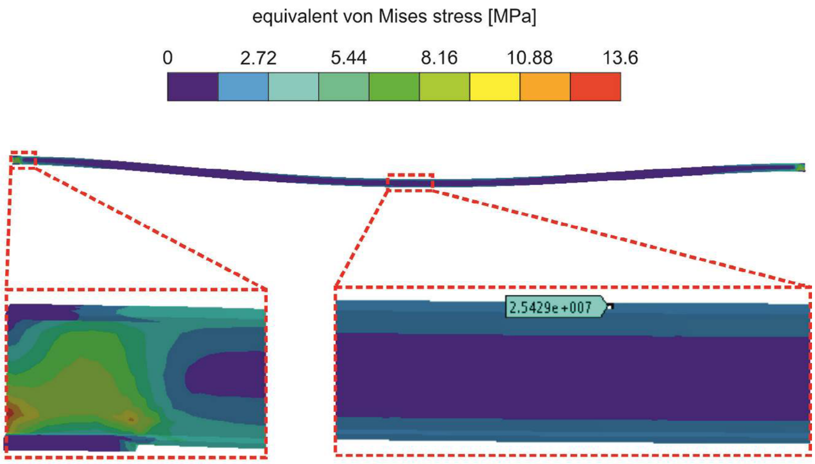

Figure 18: Developing field of von Mises equivalent stresses in the IPE 200 beam

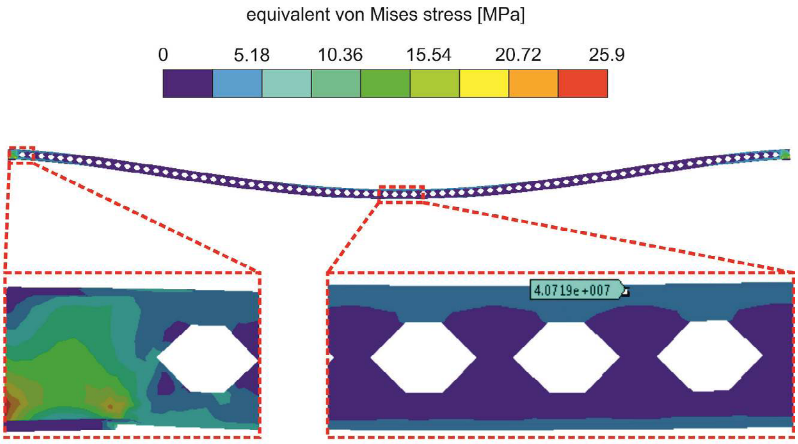

Figure 19: Developing field of von Mises equilibrium in the modified beam

Conclusions

The FEM results summarized in the diagrams of Figure 20 indicate the possibility of optimizing the treatment of the beams. Possible modification of the shape of the hole can substantially vary the results and therefore optimized processing is likely to lead to a further increase in mechanical strength of the treated beam compared to the unprocessed one.

In addition, the importance of the inspection process with non-destructive testing methods throughout the study should be noted as no exact results could be obtained if the quality of the welded samples had not been checked before they were mechanically tested. It should also be stressed that although the Finite Element method is able to provide reliable results for compound strain of complex cross-sections, these results should always be interpreted with caution and based on the initial modeling assumptions. Finally, it could be concluded that the beam treatment does not substantially affect its mechanical strength while being able to substantially facilitate the process of erecting a metal building.

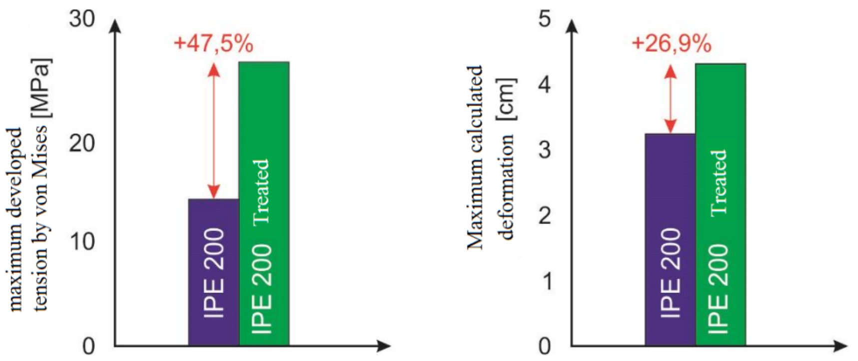

Figure 20: Variation of stress and deformation of the comparison beams

References

1. Sismanis P, Mastorakis A. Fatigue strength of concrete-reinforcing steel bars. Panhellenic Conference of Anti-Sesmic Mechanics; 2008 Nov 5-7.article 1785.
2. Tilly GP. Fatigue on steel reinforcement bars in concrete: a review. Fatigue of Engineering Materials and Structures. 1979; 2:251-268.
3. Krasnowski K. Concrete-reinforcing Steel Bars – Applications and Fatigue Tests. BIULETYN INSTYTUTU SPAWALNICTWA. 2015; 1:13-20.
4. NordTest method, STEELS FOR CONCRETE REINFORCEMENT:AXIAL LOAD FATIGUE TESTING OF BARS, NTmech 014, 1989.
5. EN 10080, Steel for the reinforcement of concrete - Weldable reinforcing steel, 2005.
6. EN 1421-3, Steel for the reinforcement of concrete – Weldable reinforcing steel – Part 3: Technical class B500C, 2007.
7. DIN 1045-1:2001-07, concrete, reinforced and pre-stressed concrete structures - Part 1: Design and construction.
8. DIN 488-1: 2009-08 Betonstahl-Teil 1: Stahlsorten, Eigenschaften, Kennzeichnung.
9. BS 4449:2005+A2:2009, Steel for the reinforcement of concrete. Weldable reinforcing steel. Bar, coil and de-coiled product.
10. Bannister J. L.: Fatigue resistance of reinforcement for concrete. Proc. Conf. Underwater Construction Technology, Department of Civil and Structural Engineering Report, University College, Cardiff; 1975.
11. Burton KT, Hognestad E. Fatigue tests on reinforcing bars - tack welding of stirrups. ACIJ. 1967; 64:244-252.
12. Walker EF, Austen IM, Harrison TC, Morley J. Fatigue and corrosion fatigue of reinforcement bars. Proc. Conf. Underwater Construction Technology, Department of Civil and Structural Engineering Report, University College, Cardiff; 1975.
13. Zienkiewicz OC, Taylor RL. The finite element method. New York (NY): McGraw-Hill; 1989.
14. Tsouknidas A, Savvakis S, Asaniotis Y, Anagnostidis K, Lontos A, Michailidis N. The effect of kyphoplasty parameters on the dynamic load transfer within the lumbar spine considering the response of a bio-realistic spine segment. Clinical Biomechanics. 2013; 28(9-10):949-955.
15. Bouzakis KD, Maliaris G, Tsouknidas A. A FEM supported semi-solid high pressure die casting process optimization based on rheological properties by isothermal compression tests at thixo temperatures extracted. Computational Materials Science. 2012; 59:133-139.
16. Bouzakis KD, Efstathiou K, Paradisiadis G, Tsouknidas A. Experimental and FEM-supported investigation of wet ceramic clay extrusion for the determination of stress distributions on the applied tools' surfaces. Journal of the European Ceramic Society. 2008; 28(11):2117-2127.
17. Bouzakis KD, Bouzakis E, Skordaris G, Makrimallakis S, Tsouknidas A, Katirtzoglou G, et al. Effect of PVD films wet micro-blasting by various Al_2O_3 grain sizes on the wear behaviour of coated tools. Surface and Coatings Technology. 2011; 205(2):S128-S132.
18. Momčilović D, Hut N, Milović L, Atanasovska I. FAILURE ANALYSIS OF CHAIN BRACKET. New Trends in Fatigue and Fracture. 2011:123-126.
19. Sujata M, Venkataswamy MA, Parameswara MA, Bhaumik SK. Failure analysis of conveyor chain links. Engineering Failure Analysis. 2006;13(6):914–924.doi: https://doi.org/10.1016/j.engfailanal.2005.07.002.
20. Schroeder CJ. Metallurgical Failure Analysis: Case Study of a Fractured Hitch. Technical Articles from Element experts; 2013.
21. Nur Ismalina Binti Haris. Failure analysis of conveyor chain links: A Case Study. 2013. Available from: Hhttp://eprints.uthm.edu.my/4733/1/NUR_ISMALINA_BINTI_HARIS.pdf.
22. Morrison RA. Polygonal action in chain drives. Machine Design. 1952; 24:155-159.
23. Mahalingam S. Polygonal action in chain drives.J Franklin Inst. 1958; 265(1):23-28.
24. Naji MR, Marshek KM. Experimental determination of the roller chain load distribution. ASME J Mech Trans Auto Des. 1983; 105:331-338.
25. Troedsson I, Vedmar L. A method to determine the static load distribution in a chain drive. ASME J Mech Des. 1999; 121:402-408.
26. Sadagopan P, Rudramoorthy R, Krishnamurthy R. Wear and fatigue analysis of two wheeler transmission chain. Journal of Scientific & Industrial Research. 2007; 66:912-918.
27. Mechanical Engineering Design. Joseph Shigley & Mische, editors. 6th ed. India: Tata McGraw Hill; 2003. p. 1074-1082, 1175.
28. ISO 15654:2015 - Fatigue test method for transmission precision roller chains.
29. ISO 606:2015 Short-pitch transmission precision roller and bush chains, attachments and associated chain sprockets.
30. John L. Wright. Chains for Drives and Conveyors - Lube 'Em to Last. Available from: http://www.machinerylubrication.com/Authors/Detail/813.
31. Priyanka Nandkumar Velhal. Experimental Stress Analysis and FEA Validation of chain link for 280 cc Drive International. International Engineering Research Journal. 847-855.
32. Kameda J, Nishiyama Y. Combined effects of phosphorus segregation and partial intergranular fracture on the ductile–brittle transition temperature in structural alloy steels. Materials Science and Engineering: A. 2011; 528(10–11):3705–3713.
33. ErhartH, Grabke HJ. Equilibrium segregation of phosphorus at grain boundaries of Fe–P, Fe–C–P, Fe–Cr–P, and Fe–Cr–C–P alloys. Metal Science. 1981; 15(9):401-408.
34. Kanvinde AM, Deierlein GG. Finite-Element Simulation of Ductile Fracture in Reduced Section Pull-Plates Using Micromechanics-Based Fracture Models. Journal of Structural Engineering. 2007; 133(5):656–664.
35. Olabi AG, Lorza RL, Benyounis KY. Quality Control in Welding Process. Comprehensive Materials Processing. 2014; 6:193-212.
36. Ghaffari B, Mozurkewich G. Non-Destructive Evaluation of Spot-Weld Quality. Failure Mechanisms of Advanced Welding Processes. 2010:101-136.
37. Matos CG, Dodds JRH. Probabilistic Modeling of Weld Fracture in Steel Frame Connections Part I: Quasi-Static Loading. Engineering Structures. 2001; 23(8):1011–1030.
38. Ditchburn RJ, Burke SK, ScalaCM. NDT of Welds: State of the Art. NDT & E International. 1996; 29(2):111-117.

39. Arakawa T, Hirose S, Senda T. The Detection of Weld Cracks Using Ultrasonic Testing. NDT International. 1985; 18(1):9-117.
40. Huang X, Tong L, Zhou F, Chen Y. Prediction of Fracture Behavior of Beam-to-Column Welded Joints Using Micromechanics Damage Model. Journal of Constructional Steel Research. 2013; 85:60–72.
41. Wang YQ, Zhou H, Shi YJ, Xiong J. Fracture Prediction of Welded Steel Connections Using Traditional Fracture Mechanics and Calibrated Micromechanics Based Models. International Journal of Steel Structures. 2011; 11(3):351–366.
42. Wang YQ, Zhou H, Shi YJ, Xiong J. Fracture Behavior Analyses of Welded Beam-to-Column Connections Based on Elastic and Inelastic Fracture Mechanics.International Journal of Steel Structures. 2010; 10(3):253–265.